Redundancy Resolution of a Human Arm for Controlling a Seven DOF wearable Robotic System

Hyunchul Kim, Levi Makaio Miller, Aimen Al-Refai, Moshe Brand, and Jacob Rosen

***Abstract*— The human arm including the shoulder, elbow, wrist joints and exclusion scapular motion has 7 Degrees of Freedom (DOF) while positioning of the wrist in space and orientating the palm is a task that requires 6 DOF. As such it includes one more DOF than is needed to complete the task. Given the redundant nature of the arm, multiple arm configurations can be used to complete a task, which is expressed mathematically by none unique solution for the inverse kinematics. Despite this mathematical difficulty, the motor control provides a unique solution for the arm redundancy as the arm is moved in space. Resolving this redundancy is becoming critical as the human interacts with a wearable robotic system(exoskeleton) which includes the same redundancy as the human arm. Therefore, the inverse kinematics solution resolving the redundancy of these two coupled systems must be identical in order to guarantee an seamless integration. The redundancy of the arm can be formulated kinematically by defining the swivel angle - the rotation angle of the plane including the upper and lower arm around a virtual axis connecting the shoulder and wrist joints which are fixed in space. Analyzing reaching tasks recorded with a motion capture lab indicates that the swivel angle is selected such that when the elbow joint is flexed, the palm points the head. Based on these experimental results, selecting the point around the center of the head as a stationary target allows to calculate the swivel angle and in that way to resolve the human arm redundancy. Experimental results indicated that by using the proposed redundancy resolution criteria the error between the predicted swivel angle and the actual swivel angle adopted by the motor control system is less then 5 Deg. This criterion or a synthesis of several additional criteria may improve the synergistic relationships between an operator and a wearable robotic system.**

I. INTRODUCTION

The human arm including the shoulder, elbow, wrist joints and exclusion scapular motion has 7 Degrees of Freedom(DOF) while positioning of the wrist in space and orientating the palm is a task that requires 6 DOF. As such it includes one more DOF than is needed to complete the task. Given the redundant nature of the arm, multiple arm configurations can be used to complete a task, which is expressed mathematically by none unique solution for the inverse kinematics. Despite this mathematical difficulty, the motor control provides a unique solution for the arm redundancy as the arm is moved in space. Resolving this redundancy is becoming critical as the human interacts with a wearable robotic system(exoskeleton)[1] which includes the same redundancy as the human arm. Therefore, the inverse kinematics solution resolving the redundancy of these two coupled systems must be identical in order to guarantee an seamless integration [2]. Several criteria were previously developed to resolve the human arm redundancy based on minimizing work and energy [3][4] or based on a desired hand posture given target location[5][6]. Criteria for redundancy resolution may be subject to two main deficiency: (1) high level of computational power required for real time implementation into a control system of a wearable robot and (2) numerical instability due to the nature of ill-posed inverse problems. This reported research effort presents a stable and computationally efficient criterion for resolving the human arm redundancy.

Hyunchul Kim is with Dept. of Electrical Engineering, University of California Santa Cruz, Santa Cruz, CA 95064, USA hyunchul@soe.ucsc.edu

Levi Makaio Miller is with Dept. of Mechanical Engineering, University of Washington, Seattle WA, USA makaio@uw.edu

Aimen Al-Refai is with the Dept. of Computer Engineering, University of California Santa Cruz, Santa Cruz, CA 95064, USA aalrefai@soe.ucsc.edu

Moshe Brand is with the Dept. of Mechanical Engineering and Mechatronics, Ariel University Center of Samaria, Ariel, Israel mosheb@ariel.ac.il

Jacob Rosen is with the Dept. of Computer Engineering, University of California Santa Cruz, Santa Cruz, CA 95064, USA rosen@ucsc.edu

Bionics Lab https://bionics.soe.ucsc.edu/

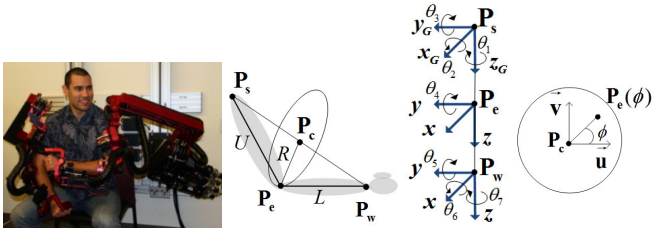

Fig. 1. a)EXO-UL7 - A 7-DOF upper limb exoskeleton [2] supports 95% of the workspace in activities of daily living b) A model of the human arm along with a definition of the virtual rotating axis which passes through the shoulder (P_c) and the wrist (P_w) joint. A circular plane with a radius R perpendicular to the axis define the location of the elbow joint (P_e) c) Definition of the coordinate systems. d) The circle depicted in 1b is redrawn along with the swivel angle ϕ

II. HUMAN ARM MODEL

A. Human Arm Model and Exoskeleton Design

The kinematics and dynamics of the human arm during activities of daily living were previously studied[8] in order to determine in part the specifications for the exoskeleton design[Fig.1(a)] - [2]. The human arm is modeled as rigid links connected by three joints: shoulder joint, elbow joint and wrist joint [1(c)][9] while neglecting the scapular and clavicle motions [10][11]. The three anatomical joints include 7 DOF (shoulder joint - 3 DOF, elbow joint - 1 DOF and, wrist joint 3 DOF) creating a redundant 7-DOF model of the entire arm.

B. The Redundant Degree of Freedom

At any point in time, the arm forms a triangle defined by the position (P_s) the position of the elbow (P_e) and the position of the wrist (P_w). Given the spherical nature of the shoulder and wrist joints (ball and socket), elbow P_e is allowed to rotate around the axis defined by the vector $(P_w - P_s)$ [Fig. 1(b)]. A local coordinate system is located at the center of the circle defined by the circular motion of the elbow (P_c). In this local coordinate system, the swivel (ϕ_{act}) defines the location of the elbow assuming the radius is fixed in length for a given position of the shoulder and the wrist joints. Let $\vec{n} = (P_w - P_s)/||P_w - P_s||$ be a normalized vector that points in

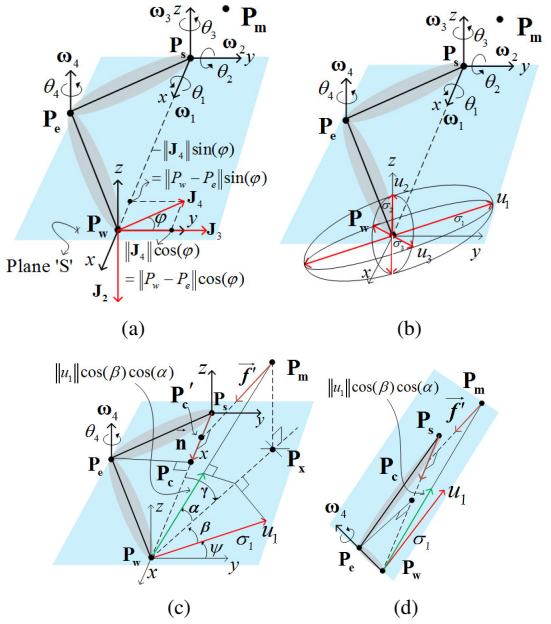

Fig. 2. Body coordinate system composed of P_w, P_e, P_s and P_m

the same direction as $(P_w - P_s)$. Let $\vec{a}$ be a unit vector in a plane normal to vector $\vec{n}$.

$$\vec{u} = (\vec{a} - (\vec{a}\cdot\vec{n})\vec{n}) / ||\vec{a} - (\vec{a}\cdot\vec{n})\vec{n}|| \tag{1}$$

where $\vec{a}$ can be selected as vector pointing to an arbitrary direction. Badler[12] suggested $\vec{a}$ to point along the vertical direction along the $\vec{z}$ axis. The last vector of an orthogonal coordinate system ($\vec{v}$), is defined as a result of a cross product of $\vec{n}$ with $\vec{u}$. Vectors $\vec{n}$, $\vec{u}$ and $\vec{v}$ form an orthonormal coordinate system. Where $\vec{u}$ and $\vec{v}$ are in the circular plane of the elbow [Fig. 1(d)]. Using geometrical consideration, the radius (R) and center (P_c) of the circle are found to be

$$R = U\sin(\alpha), \quad P_c = P_s + U\cos(\alpha)\cdot\vec{n} \tag{2}$$

$$\cos(\alpha) = \frac{U^2 - L^2 - ||P_w - P_s||^2}{-2L||P_w - P_s||} \tag{3}$$

where U and L are the length of the upper and lower arm segments[Fig. 1(b)]. The position of the elbow can now be expresses as a function of ϕ_{act} [13].

$$P_e = R[\cos(\phi_{act})\vec{u} + \sin(\phi_{act})\vec{v}] + P_c \tag{4}$$

Specifying the swivel angle resolves the redundancy [12] and all the joint angles can be defined by solving the following two equations.

$$T_1T_2T_3T_4T_5T_6T_7g_{st} = g_d, \quad T_1T_2P_{e_o} = P_e(\phi_{act}) \tag{5}$$

where T_i is the 4×4 homogeneous transformation matrix from the link frame $i-1$ to i. g_{st} is the transformation matrix from the 7th link frame to the end effector frame. g_d is the homogeneous transformation matrix that represents the end effector position and orientation. P_{e_o} is the initial position of the elbow, and $P_e(\phi_{act})$ is position of the elbow and defined by equation (4). This set of equations provide straight forward and unique solution to the inverse kinematic problem [12].

III. Swivel Angle Estimation

Given the role of the head as a cluster of sensing organs and the importance of the arm manipulation to deliver food to the mouth, we hypothesized that the swivel angle is selected by the motor control system to efficiently retract the palm to the head region. It implies that during the arm movement toward an actual target, the virtual target point on the head is also set to efficiently retract palm to the virtual target.

A. Manipulability Ellipsoid

Due to the concept of the efficient arm movement in the Hypothesis, the human arm configuration based on this Hypothesis can be closely associated with manipulability ellipsoid. Let P_m denote the virtual target position around mouth in Fig.2(a). When we consider the various combinations of joint velocities satisfying the condition in which $\Sigma_{i=1}^{n}\dot{\theta_i}^2 = 1$, the hand velocity as a function of the joint velocity is described by an ellipsoid that defines the arm's scaled Jacobian. The largest among the major axes of the manipulability ellipsoid defines the best mapping between the joint space and the end effector (hand) space. It is therefore the direction in which the hand is more likely to move [14] - Fig.2(b). Assuming that virtual hand movement follows the shortest path connecting P_w to P_m, the swivel angle is chosen such that the projection of major axis of the manipulability ellipsoid onto $(P_w - P_m)$ will be maximized.

Lemma 3.1: Given the inequality $\|P_w - P_s\| > \|P_w - P_e\|$, the longest axis of the manipulability ellipsoid is coplanar with plane S, defined by P_w, P_e and P_s, and its magnitude σ_1 is expressed as

$$\sigma_1 = \sqrt{\lambda_1} = \sqrt{\left(\left(L_{ws}^2 + L_{we}^2\right) + \left(L_{ws}^2 + L_{we}^2\right)c_1\right)/2} \tag{6}$$

$$c_1 = \sqrt{1 - c_2}, \; c_2 = 4L_{we}^2L_{ws}^2\sin(\varphi)^2 / \left(L_{ws}^2 + L_{we}^2\right)^2$$

Proof: Define a new frame with an origin located at P_s as shown in Fig.2(a). The z axis of the frame is orthogonal to the plane 'S' and the x axis is defined along the vector $(P_w - P_s)$. The relationship between the end effector velocity $\dot{\mathbf{P}} = [\dot{P_{wx}}\ \dot{P_{wy}}\ \dot{P_{wz}}]^T$ and the joint velocity $\dot{\theta}_{1234} = [\dot{\theta_1}\ \dot{\theta_2}\ \dot{\theta_3}\ \dot{\theta_4}]$ is defined as follows

$$\dot{\mathbf{P}} = \mathbf{J}\dot{\theta}_{1234} = [\mathbf{J}_1\ \mathbf{J}_2\ \mathbf{J}_3\ \mathbf{J}_4]\dot{\theta}_{1234} \tag{7}$$

$$= \mathbf{J}_1\dot{\theta_1} + \mathbf{J}_2\dot{\theta_2} + \mathbf{J}_3\dot{\theta_3} + \mathbf{J}_4\dot{\theta_4} \tag{8}$$

$$= \mathbf{J}_2\dot{\theta_2} + \mathbf{J}_3\dot{\theta_3} + \mathbf{J}_4\dot{\theta_4} = [\mathbf{J}_2\ \mathbf{J}_3\ \mathbf{J}_4]\dot{\theta}_{234} \tag{9}$$

$$\mathbf{J}_i = \begin{cases} w_i \times (P_w - P_s), i = 1,2,3 \\ w_i \times (P_w - P_e), i = 4 \end{cases} \tag{10}$$

where $\mathbf{J}_1 = w_1 \times (P_w - P_s) = \vec{x} \times (P_w - P_s) = 0$ in Eq. 8. By introducing a new variable φ for $\mathbf{J}_4$ and using the fact that $w_2 = \vec{y}$ and $w_3 = \vec{z}$ in Fig.2(a), we have

$$\mathbf{J}_2 = \|P_w - P_s\|[0\ 0\ -1]^T, \; \mathbf{J}_3 = \|P_w - P_s\|[0\ 1\ 0]^T \tag{11}$$

$$\mathbf{J}_4 = \|P_w - P_e\|[-\sin(\varphi)\ \cos(\varphi)\ 0]^T \tag{12}$$

Substituting J_2 and J_4 defined by Eq.11 and 12 into Eq.9 results in

$$\dot{\mathbf{P}} = \begin{pmatrix} 0 & 0 & -L_{we}\sin(\varphi) \\ 0 & L_{ws} & L_{we}\cos(\varphi) \\ -L_{ws} & 0 & 0 \end{pmatrix} \dot{\theta}_{234} = \mathbf{J}_{234}\dot{\theta}_{234} \tag{13}$$

where $L_{ws} = \|P_w - P_s\|$ and $L_{we} = \|P_w - P_e\|$. According to the singular value decomposition, $\mathbf{J}_{234}$ can be represented as $\mathbf{J}_{234} = \mathbf{U}\mathbf{D}\mathbf{V}^T$ where $\mathbf{U} = [u_1\ u_2\ u_3]$, $\mathbf{V} = [v_1\ v_2\ v_3]$ and $\mathbf{D} = diag[\sigma_1\ \sigma_2\ \sigma_3]$. The vectors u_i in $\mathbf{U}$ define the three axes of the manipulability ellipsoid and the vectors σ_i in $\mathbf{D}$ define the magnitude of the u_i as depicted in Fig.2(b). Note that u_i and σ_i are eigenvectors and square root of the non-zero eigenvalues of $\mathbf{J}_{234}\cdot\mathbf{J}_{234}^*$. The equation $\det\left(\mathbf{J}_{234}\cdot\mathbf{J}_{234}^* - \lambda\mathbf{I}\right) = 0$ is solved to obtain u_i and σ_i. According to Sarrus's rule,

$$\lambda_{1,2} = \left(\left(L_{ws}^2+L_{we}^2\right) \pm \left(L_{ws}^2+L_{we}^2\right)c_1\right)/2\ ,\ (\lambda_1>\lambda_2) \quad (14)$$

$$c_1=\sqrt{1-c_2},\ c_2=4L_{we}^2L_{ws}^2\sin(\varphi)^2/\left(L_{ws}^2+L_{we}^2\right)^2$$

$$\lambda_3 = L_{ws}^2 \quad (15)$$

in which $c_2 \leq 1$ and $c_1 \leq 1$. Thus $\lambda_{1,2}$ are not complex numbers. When $L_{ws} \geq L_{we}$ which covers most of the human arm workspace fir which $\lambda_1 \geq \lambda_3 \geq \lambda_2$.

$$(\mathbf{J}_{234}\cdot\mathbf{J}_{234}^*)\mathbf{X}=\lambda\mathbf{X},\quad \mathbf{X}=[x\ y\ z]^T \quad (16)$$

Since only the longest axis of the manipulability ellipsoid is of interest, the eigen vector u_1 is computed by applying the corresponding eigen value λ_1 to λ in Eq.16 and defined as

$$y=\frac{\lambda_1+L_{we}^2\sin(\varphi)\cos(\varphi)}{-L_{we}^2\sin(\varphi)^2}x=\left(-\frac{\lambda_1}{L_{we}^2\sin(\varphi)^2}-\frac{1}{\tan(\varphi)}\right)x \quad (17)$$

Note that the slope in Eq.17 is negative since $\lambda_1>0$ and $0<\varphi\leq\phi/2$. When $\varphi=0$, the arm is in the singular configuration. Therefore the vector u_1 is placed as shown in Fig.2(c) and coplanar with plane S. ■

B. Optimum Swivel angle

The optimum swivel angle is defined such that the projection of the longest axis u_1 on the vector P_w-P_s is maximized for the given wrist position.

$$\phi = \underset{\alpha,\beta\in[0\ \pi/2]}{\arg\max}\ [u_1^T(P_w-P_s)] \quad (18)$$

$$= \underset{\alpha,\beta\in[0\ \pi/2]}{\arg\max}\ [\|u_1\|\|P_w-P_s\|\cos(\alpha)\cos(\beta)] \quad (19)$$

where α and β are the angles between (P_w-P_s) and plane S, and the angle between u_1 and the projection of (P_w-P_s) onto S[Fig.2(c)] respectivly. Note that the projected portion of u_1 onto (P_w-P_s) is represented by $\|u_1\|\cos(\alpha)\cos(\beta)$ and marked as a green arrow in Fig.2(c). Based on the geometry defined in Fig.2(c), $cos(\beta)$ is defined as

$$\cos(\beta) = \cos(\pi/2-\gamma-\psi)=\sin(\gamma+\psi) \quad (20)$$

$$= c_3\sin(\gamma)+c_4\cos(\gamma) \quad (21)$$

$$= \frac{c_3||P_x-P_c'||+c_4||P_c'-P_w||}{||P_x-P_w||} \quad (22)$$

$$= \frac{c_3||\vec{f'}\cdot\frac{P_c-P_e}{||(P_c-P_e)||}||+c_4||P_c'-P_w||}{||P_x-P_w||} \quad (23)$$

$$= \frac{c_3||\vec{f'}||\cos(\eta)+c_4||P_c'-P_w||}{||P_x-P_w||} \quad (24)$$

where c_3 and c_4 mean $\cos(\psi)$ and $\sin(\psi)$ individually. Eq.20 comes from the fact that $(\gamma+\psi)\leq\pi/2$ and η in Eq.24 is the angle between $\vec{f'}$ and (P_c-P_e). Since $\cos(\alpha)=||P_x-P_w||/||P_m-P_w||$,

$$\cos(\alpha)\cos(\beta) = \frac{||P_x-P_w||}{||P_m-P_w||}\cdot\frac{c_3||\vec{f'}||\cos(\eta)+c_4||P_c'-P_w||}{||P_x-P_w||}$$

$$= \frac{c_3||\vec{f'}||\cos(\eta)+c_4||P_c'-P_w||}{||P_m-P_w||} \quad (25)$$

$$= c_5\cos(\eta)+c_6 \quad (26)$$

where constants c_5 and c_6 are $c_3||\vec{f'}||||P_m-P_w||$ and $c_4||P_c'-P_w||||P_m-P_w||$. Substituting the expression for $cos(\alpha)\cos(\beta)$ in Eq.26 into Eq.19 results in

$$\phi = \underset{\alpha,\beta\in[0\ \pi/2]}{\arg\max} = [\|u_1\|\|P_w-P_s\|(c_3\cos(\eta)+c_4)] \quad (27)$$

When $\eta=0$, ϕ defined in Eq.27 is maximized and $\alpha=0$ in Eq.19. In this condition, plane S is coplanar with the plane composed by P_m, P_s and P_w as shown in Fig.2(d). Then the swivel angle is calculated given the known positions P_m, P_w and P_s. In order to do so a new vector $\vec{f}=P_w-P_m$ is defined. The vector $\vec{f'}$, is the projection of $\vec{f}$ on along the direction of P_w-P_s in Fig.2(c). Based on the fact that $\vec{f'}$ is parallel to vector $P_e(\phi)-P_c$ when $\alpha=0$, the swivel angle is estimated by

$$\phi_{est}=\arctan 2\left(\vec{n}\cdot\left(\vec{f'}\times\vec{u}\right),\vec{f'}\cdot\vec{u}\right) \quad (28)$$

The estimation algorithm is based on a real time solution of the inverse kinematic. The accuracy of the ϕ_{est} estimation was assessed based on experimental results described in the following section.

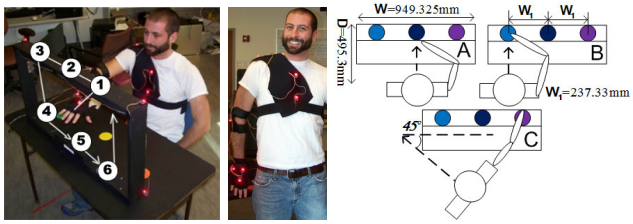

(a) (b) (c)

Fig. 3. a) Hand trajectory for data collection b) Positions of LED markers: Shoulder(Acromioclavicular joint), Elbow(Lateral edge of the Ulna), Wrist(Medial & Lateral edge of the distal end of the radius & ulna), Palm(between 2 & 3 metacarples) and Torso(Upper & lower sternum) c) Top view of three different tasks. Height of table-top to top-of-shelf = 501.65mm, Height of table-top from ground = 736.6mm.

IV. Experimental Protocol and Results

A. Experimental Setup and Protocol

The experimental setup is shown in Fig.3. The kinematic data of the human arm is collected using the motion capture system(Phasespace, Inc.) equipped with eight cameras providing a 240Hz sampling rate and millimeter accuracy at a distance of three meters. Active LED makers were attached to a key anatomical locations which are the shoulder, elbow, wrist and chest [Fig.3]. Five right handed healthy subjects(three male and two female subjects with an average height of 175 cm and an average age of 29) participated in the experiment. The subjects were instructed to place their hands at the center of the task space and reach the targets in a sequential order at a self directed pace as follows[Fig.3(c)].

$$Center\rightarrow 1\rightarrow 2\rightarrow 3\rightarrow 4\rightarrow 5\rightarrow 6(5repetitions)$$

Each subject completed five repetitions of the protocol under three experimental conditions. In each experimental condition the the 6 points frame was aligned differently with respect to the subject's torso and aimed to cover the majority of the right arm workspace - see Fig.3(a) for details.

B. Optimal Estimation of Target Location - P_m

Due to anthropometric differences between the subjects, it is desired to locate optimal location of of the target - P_m for each subject. An LED marker located on the chest P_{ch} was used to estimate the target location - P_m. In this experiment the orientation of the torso was restricted as a result that the position of the P_m as a function of time is represented by

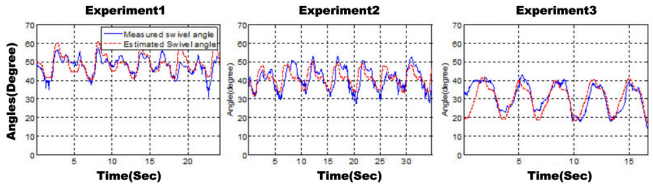

(a)

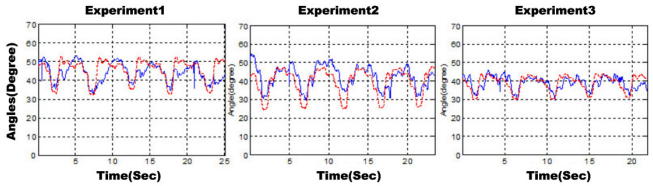

(b)

Fig. 4. Comparison between estimated swivel angle(Red dotted line) and measured swivel angle(Blue line) for two subjects

$$P_m(t) = P_{ch}(t) + P_o \tag{29}$$

where P_o is the fixed translation from P_{ch} with respect the global frame. The optimal value of P_o is selected such that the difference between $\phi(t)_{est}$ - the estimated swivel angle based on Eq.28 and $\phi(t)_{act}$ - the calculated swivel angle based on the measured joint positions is minimized.

$$P_o\left(x_{opt}, y_{center}, z_{opt}\right) = \arg\min_{y,z \in U_s} \frac{1}{T} \int_{t_x}^{t_x+T} |\phi(t)_{act} - \phi(t)_{est}| dt \tag{30}$$

where U_s and y_{center} in Eq.30 coresponds to the (x,z) coordinates in the Sagittal plane and the y coordinate is taken from $P_{ch}(t)$. For each data set only the first set of data (a complete circle) was used for fitting P_o. The actual P_o used for subjects are summarized in Table I. It shows that estimated P_m with respect to the chest position is located on the face as we expected.

TABLE I
ESTIMATION ERROR

Subject	$P_o(mm)$ (x_{opt}, z_{opt})	Standard Deviation of Error Exp 1	Exp 2	Exp 3	Mean error
1	(-160,280)	2.344°	2.720°	3.769°	3.024°
2	(-140,320)	2.337°	2.579°	1.365°	3.516°
3	(-70,290)	3.395°	2.756°	2.340°	4.103°
4	(-140,330)	2.817°	2.564°	3.010°	3.525°
5	(-60,220)	2.740°	3.225°	3.501°	4.739°

C. Swivel Angle Estimation

The swivel angles were estimated based on the wrist position data recorded during the experiment and the proposed redundancy resolution criterion. The estimated swivel angles were then compared with calculated swivel angles indicated by the the motor control system of the subjects. The standard deviation of the estimation errors are listed along the absolute error mean across all the subjects in Table.I. The results indicated the the standard deviations are less than five degrees. Note that the results in experiment 1 - Fig.4 indicate weaker correlation. This is due to the fact that left hand side targets were at the left edge of the right arm workspace, a situation that resulted in torsional movement and led to larger errors in predicting the swivel angle .

V. CONCLUSION

Given a reaching task $(6DOF)$ the human arm is considered to be a redundant serial articulated mechanism $(7DOF)$. The human motor control resolves the arm redundancy however the criteria used for this resolution are not fully understood. A swivel angle was defined in order to express mathematically the the redundant DOF and a criterion was defined for estimating the value of the swivel angle for any given position and orientation of the hand. According to the proposed criterion, for any given arm configuration, the swivel angle is selected such that by flexing the elbow joint the palm reaches the head. This criterion was studied experimentally showing that the difference between prediction of the swivel angle and the one selected naturally by the motor control system was less the 5 deg. The proposed mathematical formulation including the swivel angle and the criterion for the redundancy resolution provides a closed form solution for the human arm inverse kinematics. As such it is suitable for real-time control of an 7 DOF upper limb wearable robotic system (exoskeleton) which requiring both precision and efficiency [8]. Additional applications of the proposed algorithm may be in computer animation of the human arm movements. The redundancy of the human arm as many other subsystem of the human body is aimed to cope with uncertainty. This uncertainty may also be related to disability. If one or more of the joints in the arm dysfunction, there are sufficient DOF left to facilitate essential functions such as eating [8].

REFERENCES

[1] J. Rosen and J. C. Perry, "Upper limb powered exoskeleton," *International Journal of Humanoid Robotics*, vol. 4, no. 3, pp. 529–548, 2007.

[2] J. C. Perry, J. Rosen, and S. Burns, "Upper-limb powered exoskeleton design," *Mechatronics*, vol. 12, no. 4, pp. 408–417, 2007.

[3] T. Kang, J. He, and S. I. H. Tillery, "Determining natural arm configuration along a reaching trajectory," *Exp Brain Res*, vol. 167, no. 3, pp. 352–361, 2005.

[4] M. A.Admiraal, M. J. Kusters, and S. C. Gielen, "Modeling kinematics and dynamics of human arm movements," *Motor Control*, vol. 8, no. 3, pp. 312–338, 2004.

[5] C. Gielen, E. J. Vrijenhoek, T. Flash, and S. Neggers., "Arm position constraints during pointing and reaching in 3-d space," *Journal of Neurophysiology*, vol. 78(2), pp. 660–673, 1997.

[6] ——, "Review of models for the generation of multi-joint movements in 3-d," *Advances in experimental medicine and biology, Progress in Motor Control*, vol. 629, pp. 523–550, 2009.

[7] P. J. C and J. Rosen, "Design of a 7 degree-of-freedom upper-limb powered exoskeleton," in *Proceedings of the 2006 BioRob Conference, Pisa, Italy*, February 2006, pp. 5081–5084.

[8] P. Joel, J. Powell, and J. Rosen, "Isotropy of an upper limb exoskeleton and the kinematics and dynamics of the human arm," *Journal of Applied Bionics and Biomechanics*, vol. 6, no. 2, pp. 175–191, 2009.

[9] J. U. Korein, *A Geometric Investigation of Reach*. MIT Press, 1985.

[10] P. Culmer, A. Jackson, M. Levesley, J. Savage, R.Richardson, J. Cozens, and B. Bhakta, "An admittance control scheme for a robotic upper-limb stroke rehabilitation system," in *Engineering in Medicine and Biology 27th Annual Conference*, 2005, pp. 5081–5084.

[11] W. Maurel, "3d modeling of the human upper limb including the biomechanics of joints, muscles amd soft tissues," Ph.D. dissertation, Ecole Polytechnique Federale de Lausanne, 1998, these No 1906.

[12] N. I. Badler and D. Tolani, "Real-time inverse kinematics of the human arm," *Presence*, vol. 5, no. 4, pp. 393–401, 1996.

[13] D. Tolani, A. Goswami, and N. I. Badler, "Real-time inverse kinematics techniques for anthropomorphic limbs," *Graphical Models and Image Processing*, vol. 62, no. 5, pp. 353–388, Sept. 2000.

[14] A. A. Maciejewski, "Dealing wit the ill-conditioned equations of motion for articulated figures," *IEEE Computer Graphics and Applications*, pp. 63–71, 1990.